This article has been accepted for publication in a future issue of this journal, but has not been fully edited. Content may change prior to final publication. Citation information: DOI 10.1109/JIOT.2018.2790578, IEEE Internet of Things Journal

Distributed Wireless Power Transfer System for Internet-of-Things Devices

Kae Won Choi, *Senior Member, IEEE*, Arif Abdul Aziz, Dedi Setiawan, Nguyen Minh Tran, Lorenz Ginting, and Dong In Kim, *Senior Member, IEEE*

***Abstract*—The wireless power transfer via an electro-magnetic (EM) wave enables far-field power transfer for supplying power to IoT devices. However, the power attenuation of the EM wave leads to low end-to-end power transfer efficiency. In this paper, we provide an analytic and experimental study on the distributed wireless power transfer system as a means to overcome the low power transfer efficiency. In the distributed wireless power transfer system, a number of multi-antenna power beacons, which are distributed over space, send out wireless power to charge IoT devices. Since each power beacon has a separate local oscillator and controller, it is very challenging to achieve frequency and phase synchronization among power beacons, which is the prerequisite for optimal distributed beamforming. In this paper, we study the performance of the distributed wireless power transfer system with or without the frequency and phase synchronization. Based on the experiment and simulation results, we show that the distributed wireless charging is advantageous in terms of the coverage probability as long as the optimal distributed beamforming is available in the distributed wireless power transfer system.**

***Index Terms*—Wireless power transfer, IoT devices, distributed antenna system, wireless-powered sensor networks, coverage probability, energy harvesting**

I. Introduction

Recently, the wireless power transfer via an electro-magnetic (EM) wave has gained a lot of attention thanks to its capability of far-field power transmission [1]. Differently from magnetic wireless power transfer techniques such as inductive coupling and magnetic resonant coupling, the RF energy transfer technique makes use of a radiative EM wave to convey power through a free space. Therefore, the RF energy transfer enjoys an advantage of relatively longer energy transfer distance compared to magnetic wireless power transfer [2]. However, the wireless power transfer via an EM wave suffers from low end-to-end transfer efficiency because of severe power attenuation. One viable solution to overcome this problem in indoor environment is to use a distributed antenna system [1], [3]. The multi-antenna system with collocated antennas can efficiently transfer energy only to a limited area close to the antennas. On the other hand, the distributed antennas surrounding the target area can cover the whole area, eliminating blind spots around which no nearby antenna is present.

The distributed wireless power transfer system has been theoretically studied by some works (e.g., [4]–[7]). The authors of [4] have proposed simultaneous wireless information and power transfer (SWIPT) and energy cooperation in a multiple-input single-output (MISO) distributed antenna system. In [5], the authors have studied the resource allocation algorithm for the distributed antenna-based SWIPT. In [6], the authors have characterized the achievable rate-energy tradeoff in a multi-user SWIPT system with distributed transmitters. The work [7] has discussed the research trend and the potential architecture of the distributed version of the massive multiple-input multiple-output (MIMO) technology for SWIPT.

Other than those theoretical works, few experimental researches regarding the wireless power transfer with the distributed antennas have been conducted (e.g., [8]–[12]). In [8], the ubiquitous power source with a magnetron and a slotted antenna array has been implemented in a shield room, and a mobile phone has been successfully charged with microwave power everywhere in the room. In [9], the distributed retro-reflective beamforming for the wireless power transfer is experimentally verified. The work [10] has demonstrated the constructive and destructive energy aggregation at the power receiver. In [11], the distributed medium access control (MAC) protocol for wireless power transfer is proposed. In this MAC protocol, the two-tone energy transfer is suggested to mitigate the negative effect of the phase mismatch between the signals from multiple energy transmitters. In [12], the authors have proposed the carrier shift diversity (CSD) for multi-point wireless power transmission, which assigns slightly different frequencies to multiple transmitters.

In this paper, we consider the distributed wireless power transfer system consisting of multiple separate power beacons, each of which is equipped with multiple transmit antennas. In this system, it is of great importance to perform optimal distributed beamforming to maximize the power transfer efficiency. The optimal distributed beamforming makes the EM waves from all antennas constructively combined at the receiver so that the receive power is maximized. The prerequisite for the optimal distributed beamforming is both the frequency and phase synchronization. Frequency drifts between different power beacons are caused by the imperfection (i.e., hardware offset) of local oscillators. For optimal beamforming, frequency drifts should be compensated by a frequency synchronization method, for example, a designated master transmitter can send the reference signal to coordinate

The authors are with the School of Information and Communication Engineering, Sungkyunkwan University (SKKU), Suwon, Korea (email: kaewonchoi@skku.edu, arif.abdul.aziz92@gmail.com, morethanubabe@gmail.com, minhtran.uet@gmail.com, lorenzgins@gmail.com, dikim@skku.ac.kr).

This work was supported in part by the National Research Foundation of Korea (NRF) grant funded by the Korean government (MSIP) (2014R1A5A1011478), and in part by the Basic Science Research Program through the NRF funded by the Korean government (MSIP) (NRF-2017R1A2B4010285).

This article has been accepted for publication in a future issue of this journal, but has not been fully edited. Content may change prior to final publication. Citation information: DOI 10.1109/JIOT.2018.2790578, IEEE Internet of Things Journal

the synchronization [13]. For the phase synchronization, each antenna should transmit a signal conjugate to the channel gain between transmit and receive antennas. If an independent controller is used in each power beacon, the phase synchronization is a challenging task. In [13] and [14], a closed-loop feedback algorithm is proposed for achieving the phase synchronization in the distributed antenna system. Although some existing methods (e.g., [13], [14]) can be used for optimal distributed beamforming, the realization of both the frequency and phase synchronization is still very costly and challenging.

In this paper, we provide an analytic and experimental study of the distributed wireless power transfer with or without the frequency and phase synchronization. We consider three beamforming schemes: optimal, static, and random beamforming. The optimal beamforming scheme can be used only when the frequency and phase synchronization is achieved. If the phase synchronization is not available, we can use the static beamforming scheme that simply fixes the phases of the transmit signals. However, this static beamforming can cause the signals to be destructively combined in many places. This problem can be solved by using the random beamforming that randomizes the phases of the transmit signals. The focus of this paper is not to design the beamforming schemes but to analyze the performance of them. In this paper, we analyze the average receive power when the optimal, static, and random beamforming schemes are applied between multiple antennas within each power beacon or across multiple power beacons. In addition, we analyze the coverage probability, which is defined as the probability that the receive power is not less than a given threshold.

We have built a real-life testbed for the distributed wireless power transfer. For implementing the multi-antenna power beacon, we have designed and fabricated a phased antenna array board with 16 transmit paths, each of which consists of a phase shifter, a variable attenuator, and an amplifier. In addition, we have implemented a low power IoT device that is capable of receiving the radio frequency (RF) wireless power. The IoT device consists of off-the-shelf components such as a rectifier, an energy storage, a voltage regulator, a microcontroller unit (MCU), and an RF transceiver. In the testbed, the power beacons and the IoT device are fully integrated to perform the optimal, static, and random beamforming in real time. We have conducted extensive experiments to show the receive power all over the testbed space and the coverage probabilities when various beamforming schemes are used. We show that the analysis on the receive power and the coverage probability very well agrees with the experimental results. We also show that the distributed wireless charging is advantageous in terms of the coverage probability in comparison to a single power beacon with multiple collocated antennas, as long as the optimal distributed beamforming is available.

It is noted that this paper is the extended version of our previous conference paper [15]. Compared to the conference paper, this paper establishes more elaborated system model (e.g., EM wave propagation model and low power IoT device model), includes detailed discussion on the hardware architectures for distributed wireless power transmitters, provides more advanced mathematical analysis, and presents extensive experimental and simulation results.

In summary, the contributions of this paper are twofold.

- We suggest the optimal, static, and random beamforming schemes for the distributed wireless power transfer in consideration of the practical limitation in a hardware capability. We provide the analysis for these beamforming schemes in terms of the receive power and the coverage probability. The existing theoretical works (e.g., [4]–[7]) do not consider all of these beamforming schemes since they assume the perfect knowledge on the channel state information.
- We present extensive experimental results obtained from a real-life testbed for the multi-antenna distributed wireless power transfer with the optimal, static, random beamforming, and verify that the analysis well matches with the experimental results. No previous experimental work (e.g., [8]–[12]) has conducted such comprehensive experiments.

The rest of paper is organized as follows. We present the system model for the distributed wireless power transfer in Section II. We explain the possible architectures of the distributed wireless power transfer system, and investigate various distributed beamforming schemes in Section III. The receive power and the coverage probability are analyzed in Section IV. Section V presents the experimental results, and Section VI concludes the paper.

II. System Model

A. Distributed Wireless Power Transfer-Based IoT System Model

In the proposed model for the distributed wireless power transfer-based IoT system, multiple power beacons emit an RF wave to wirelessly supply power to an IoT device, as depicted in Fig. 1. We assume that there are K power beacons, each of which is equipped with N transmit antennas. Hereafter, the kth power beacon and the nth antenna are simply called beacon k and antenna n, respectively. Each power beacon can perform energy beamforming by using multiple transmit antennas to focus an energy beam on the IoT device. Moreover, multiple power beacons can cooperate with each other to optimally deliver the RF power to the IoT device. The energy beamforming along with the cooperation between the power beacons will be discussed in more detail in Section III. In the proposed system model, we consider one IoT device, equipped with a single antenna for receiving the RF power from the power beacons.

Each transmit antenna in a power beacon emits an RF signal for wireless power transfer. Let f_c denote the frequency of the RF signal. The RF signal at time t, which is sent by antenna n of beacon k, is given by

$$\kappa_{k,n}(t) = \mathrm{Re}\big[x_{k,n}(t)\exp\left(j2\pi f_c t\right)\big], \tag{1}$$

where $x_{k,n}(t)$ is the baseband complex transmit signal at time t from antenna n of beacon k. The transmit signal $x_{k,n}(t)$ is determined by the distributed beamforming algorithm, which will be discussed in Section III. Actually, $\kappa_{k,n}(t)$ in (1) is the voltage signal at the antenna port. If the antenna impedance

This article has been accepted for publication in a future issue of this journal, but has not been fully edited. Content may change prior to final publication. Citation information: DOI 10.1109/JIOT.2018.2790578, IEEE Internet of Things Journal

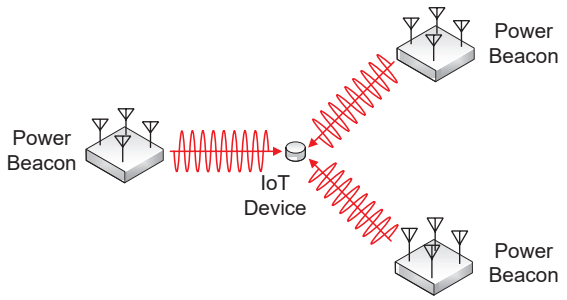

Fig. 1. Distributed wireless power transfer-based IoT system model.

is denoted by Z_0 (i.e., usually 50 Ω), the transmit power from the port of antenna n of beacon k is

$$p_{k,n}(t) = \frac{|x_{k,n}(t)|^2}{2Z_0}. \tag{2}$$

The complex channel gain from antenna n of beacon k to the antenna of the IoT device is denoted by $h_{k,n}$. It is noted that the complex channel gain is equivalent to the S-parameter between the ports of the transmit and receive antennas. We will discuss the channel gain modeling in more detail in Section II-B. The RF signal at the antenna of the IoT device, received from all antennas of all power beacons, is given by

$$\nu(t) = \mathrm{Re}\big[y(t)\exp\left(j2\pi f_c t\right)\big], \tag{3}$$

where $y(t)$ is the baseband complex receive signal at time t at the antenna of the IoT device. The receive signal $y(t)$ is given by

$$y(t) = \sum_{k=1}^{K}\sum_{n=1}^{N} h_{k,n}x_{k,n}(t) = \sum_{k=1}^{K}\mathbf{h}_k^T\mathbf{x}_k(t). \tag{4}$$

In (4), $\mathbf{h}_k$ and $\mathbf{x}_k(t)$ denote the channel gain vector $\mathbf{h}_k = (h_{k,1},\ldots,h_{k,N})^T$ and the transmit signal vector $\mathbf{x}_k(t) = (x_{k,1}(t),\ldots,x_{k,N}(t))^T$, respectively. The receive power at the antenna port of the IoT device is given by

$$r(t) = \frac{|y(t)|^2}{2Z_0}. \tag{5}$$

The received RF power at the IoT device is rectified to the DC power and is used to power up the IoT device. The IoT device model will be discussed in Section II-C.

B. Electro-Magnetic Wave Propagation Model

In this subsection, we explain an EM wave propagation model for modeling the channel gain $h_{k,n}(t)$. For doing this, we first give a spatial model for the locations of the antennas of the power beacons and the IoT device. For simplicity, we confine the spatial model to a two-dimensional plane. We assume that all antennas are omni-directional dipole antennas that are vertically positioned at the same elevation in reference to the ground. Then, the location of each antenna can be described only by a two-dimensional coordinate.

Let us denote by $\mathbf{b}_k$ the two-dimensional reference coordinate of beacon k. The relative coordinate of antenna n of beacon k in reference to $\mathbf{b}_k$ is denoted by $\mathbf{a}_{k,n}$. Then, the absolute coordinate of antenna n of beacon k is $(\mathbf{b}_k + \mathbf{a}_{k,n})$. The antennas belong to one power beacon are closely located to form an antenna array. Then, the arrangement of the antenna array (e.g., linear or circular antenna array) is determined by $\mathbf{a}_{k,n}$ for $n = 1,\ldots,N$. Let us denote by $\mathbf{c}$ the coordinate of the antenna of the IoT device. Then, the distance between beacon k and the IoT device is $d_k = \|\mathbf{b}_k - \mathbf{c}\|_2$, and the distance between antenna n of beacon k and the IoT device is $d_{k,n} = \|\mathbf{b}_k + \mathbf{a}_{k,n} - \mathbf{c}\|_2$. We assume that no antenna coupling is occurred between antennas since all the antennas are separated by at least half-wavelength.

Now, we present the modeling of the channel gain from antenna n of beacon k to the IoT device (i.e., $h_{k,n}$). The wavelength of the RF signal with frequency f_c in a free space is denoted by λ. Then, the channel gain is calculated as

$$\begin{aligned} h_{k,n} &= \sqrt{L}\left(\frac{\widehat{d}}{d_{k,n}}\right)^{\frac{\alpha}{2}}\sqrt{g_t g_r}\exp\left(j2\pi\frac{d_{k,n}}{\lambda}\right) \\ &= \sqrt{\Upsilon}d_{k,n}^{-\frac{\alpha}{2}}\exp\left(j2\pi\frac{d_{k,n}}{\lambda}\right), \end{aligned} \tag{6}$$

where $\widehat{d}$ is the reference distance for the path loss, L is the attenuation at the reference distance, α is the path loss exponent, g_t is the transmit antenna gain, g_r is the receive antenna gain, and $\Upsilon = L\widehat{d}^{\alpha}g_t g_r$. If we use the Friis equation for the path loss, we have $\alpha = 2$, $L = 1$, and $\widehat{d} = \lambda/(4\pi)$.

In this paper, we use empirically-obtained values for the parameters Υ and α in (6). To obtain the parameters and to validate the channel gain model in (6), we have conducted channel gain experiments as shown in Fig. 2. In this experiment, two dipole antennas with a 3 dBi gain are separately placed by a given distance, and the S-parameter (i.e., S_{21}) between those antennas is measured by a network analyzer. In Fig. 2, we show the power attenuation (i.e., $10\log_{10}|h_{k,n}|^2 = 10\log_{10}\Upsilon - \alpha\cdot 10\log_{10}d_{k,n}$) and the phase shift (i.e., $\angle h_{k,n} = 2\pi d_{k,n}/\lambda$) according to the distance. We can observe that the phase is shifted by 2π for every full wavelength (i.e., 0.32 m for $f_c = 920$ MHz), as modeled in (6). On the other hand, the power attenuation shows irregularity because of the indoor multi-path environment. This irregularity is not described by (6) since we assume that only a direct line-of-sight (LOS) path exists in (6) for simplicity. However, the channel gain model (6) still well describes the general attenuation trends.[1] By regression, we have found the empirical parameters for the channel gain model as $\Upsilon = 4.393\times 10^{-4}$ and $\alpha = 2.051$.

Multiple antennas equipped in one power beacon form an antenna array that is capable of beamforming. Let us assume that the IoT device is located within the far-field region of the antenna array of each power beacon. Under this assumption, we can approximate (6) as

$$h_{k,n} = \sqrt{\Upsilon}d_k^{-\frac{\alpha}{2}}\exp\left(j2\pi\frac{d_k}{\lambda}\right)\exp\left(j2\pi\frac{\mathbf{a}_{k,n}\cdot(\mathbf{b}_k - \mathbf{c})}{\lambda d_k}\right), \tag{7}$$

where '$\cdot$' denotes the dot product. Recall that $\mathbf{h}_k$ denotes the channel gain vector for power beacon k such that $\mathbf{h}_k =$

[1]For the narrowband signal here, the multi-path channel can be modeled in (6) with a relatively large $\alpha > 2$.

This article has been accepted for publication in a future issue of this journal, but has not been fully edited. Content may change prior to final publication. Citation information: DOI 10.1109/JIOT.2018.2790578, IEEE Internet of Things Journal

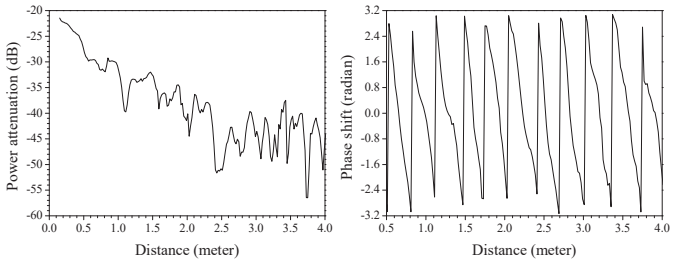

(a) Power attenuation (b) Phase shift

Fig. 2. Channel gain over distances.

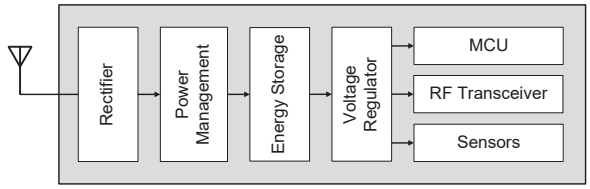

Fig. 3. Hardware architecture of the low power IoT device.

$(h_{k,1}, \ldots, h_{k,N})^T$. From (7), the channel gain vector can be written as

$$\mathbf{h}_k = \zeta_k \xi_k \boldsymbol{\psi}_k, \tag{8}$$

where $\zeta_k = \sqrt{\Upsilon} d_k^{-\frac{\alpha}{2}}$ and $\xi_k = \exp(j2\pi d_k/\lambda)$. We can see that ζ_k is a real-valued path loss depending on the distance between beacon k and the IoT device. On the other hand, ξ_k represents a phase shift caused by the distance between beacon k and the IoT device.

In (8), $\boldsymbol{\psi}_k$ is defined as an array response vector $\boldsymbol{\psi}_k = (\psi_{k,1}, \ldots, \psi_{k,N})^T$, where $\psi_{k,n} = \exp(j2\pi(\mathbf{a}_{k,n} \cdot (\mathbf{b}_k - \mathbf{c}))/(\lambda d_k))$. The array response vector $\boldsymbol{\psi}_k$ depends only on the arrangement of the antenna array (i.e., $\mathbf{a}_{k,n}$ for $n = 1, \ldots, N$) and the azimuth of the IoT device in relation to beacon k. Therefore, the array response vector $\boldsymbol{\psi}_k$ determines the antenna array beam pattern for a given transmit signal vector $\mathbf{x}_k(t)$.

C. Low Power IoT Device with RF Power Reception Capability

In this paper, we consider a low power IoT device such as a sensor node, augmented with the RF power reception capability. However, it is noted that the distributed wireless power transfer can be applied to other classes of IoT devices with higher power consumption. Fig. 3 shows the hardware architecture of the low power IoT device under consideration. The IoT device consists of an antenna for RF power reception, a rectifier, a power management circuit, an energy storage, a voltage regulator, and active components such as a microcontroller unit (MCU), an RF transceiver, and sensors.

The RF power received by the antenna is rectified to DC power by using the rectifier. The rectified DC power is stored in the energy storage through the power management circuit. The power management circuit can provide optimal impedance to the rectifier by using maximum power point tracking (MPPT) so that the rectified DC power is maximized. Recall that the receive RF power is denoted by $r(t)$. During rectification, some of the receive power is lost in the rectifier circuit or is reflected back to the antenna. Let η denote the rectifier efficiency, and then the rectified DC power is calculated as $\eta \cdot r(t)$. Typically, the rectifier efficiency is a function of the receive power $r(t)$ as well as load impedance [16]. However, an advanced multi-mode rectifier combined with the MPPT technology (e.g., Powercast P1110 used in our experiment) has quite a flat rectifier efficiency curve. Therefore, we assume that the rectifier efficiency is a constant.

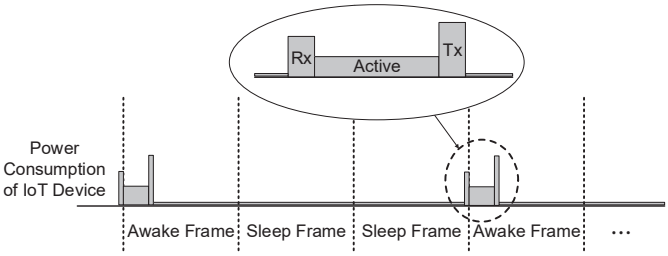

Fig. 4. Frame-based duty cycle protocol.

The energy storage can be either a rechargeable battery or a supercapacitor. In this paper, we use a supercapacitor as an energy storage for the experiments since a supercapacitor is able to withstand frequent charging and discharging cycles. The voltage regulator is the interface between the energy storage and the active components (i.e., the MCU, the RF transceiver, and the sensors), drawing energy from the energy storage to provide a stable voltage to the active components.

The active components consume the energy stored in the energy storage. Among the active components, the MCU is a processor that controls the IoT device and performs computation. The IoT device uses the RF transceiver to wirelessly communicate with the power beacon. The sensors (e.g., temperature sensor and accelerometer) obtain useful information from the environment. In a low power IoT device, it is common to alternately change the modes of those active components to reduce the power consumption. For example, we can consider four different modes: idle, active, receive, and transmit modes. In the idle mode, all active components are turned off for minimizing the power consumption, except for the timer of the MCU which wakes up the IoT device. In the active mode, the MCU and the sensors are activated for computation and sensing, while the RF transceiver is in sleep. The RF transceiver is turned on and ready for receiving data in the receive mode, and the RF transceiver transmits data while it is in the transmit mode.

The duty cycle control method determines how often the IoT device wakes up. In this paper, we consider a frame-based duty cycle control method as described in Fig. 4. Time is divided into frames. Each frame can either be a sleep frame or an awake frame. During a sleep frame, the IoT device stays in the idle mode. On the other hands, during an awake frame, the IoT device wakes up to perform sensing, computation, and communication. At the start of each awake frame, the

This article has been accepted for publication in a future issue of this journal, but has not been fully edited. Content may change prior to final publication. Citation information: DOI 10.1109/JIOT.2018.2790578, IEEE Internet of Things Journal

IoT device wakes up from the idle mode, and goes into the receive mode to receive a beacon packet from the power beacon. After the reception, the IoT device goes into the active mode to obtain information from the sensors and to perform computation. After the active mode is over, the IoT device moves on to the transmit mode to report the sensor information to the power beacon. The IoT device goes into the idle mode after the transmission is done.

The power consumption during an awake frame is much higher than that during a sleep frame. Let C_{awake} and C_{sleep} denote the power consumption during an awake frame and a sleep frame, respectively. The IoT device is able to control the average power consumption by controlling the frequency of awake frames. Let α denote the awake frame ratio that represents the ratio of awake frames to all frames. Let $\overline{C}(\alpha)$ denote the average power consumption for a given α. Then, $\overline{C}(\alpha)$ is given by

$$\begin{aligned}\overline{C}(\alpha) &= \alpha C_{\text{awake}} + (1-\alpha)C_{\text{sleep}} \\ &= (C_{\text{awake}} - C_{\text{sleep}})\alpha + C_{\text{sleep}}.\end{aligned} \tag{9}$$

As we can see in (9), the average power consumption linearly increases with the awake frame ratio α. A high awake frame ratio means that the IoT device can perform sensing, computation, and communication more frequently. However, this benefit comes at the cost of increased power consumption.

We have implemented the frame-based duty cycle control method in a real IoT device, and have measured the power consumption. The IoT device for the experiment consists of a Powercast P1110 evaluation board for receiving the RF power, a Zolertia Z1 mote with an MCU and an RF transceiver, and a custom-built power board with a voltage regulator and a supercapacitor. Fig. 3 shows the picture of the implemented IoT device. The frame length of the frame-based duty cycle control method is set to 100 ms. The IoT device randomly decides if each frame is an awake or a sleep frame according to the given awake frame ratio. The power consumption of the active components is measured by using a source meter.

In Fig. 5, we show the instantaneous power consumption of the IoT device over time. We can see that the IoT device wakes up more frequently as the awake frame ratio becomes higher, resulting in higher average power consumption. Fig. 6 shows the average power consumption as a function of the awake frame ratio. We can see the linear relationship in (9) between the average power consumption and the awake frame ratio holds. From this figure, we can obtain the parameters for (9) as $C_{\text{awake}} = 5.54$ mW and $C_{\text{sleep}} = 0.06$ mW.

The IoT device can stay alive in a long run only if the average of the rectified DC power is not lower than the average power consumption. The average receive power is given by

$$\overline{r} = \langle r(t) \rangle = \lim_{T\to\infty} \frac{1}{T} \int_0^T r(t)\ \mathrm{d}t, \tag{10}$$

where '$\langle\cdot\rangle$' denotes the time average of a signal. Then, the required average receive power for a given α is

$$\overline{r} \geq \overline{C}(\alpha)/\eta. \tag{11}$$

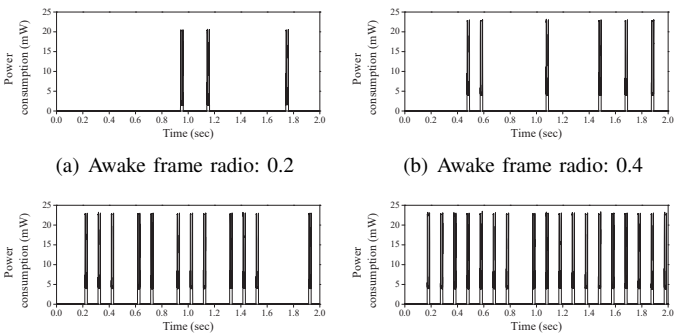

(a) Awake frame radio: 0.2 (b) Awake frame radio: 0.4

(c) Awake frame radio: 0.6 (d) Awake frame radio: 0.8

Fig. 5. Instantaneous power consumption of the IoT device.

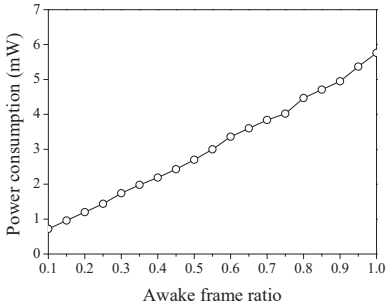

Fig. 6. Average power consumption of the IoT device according to the awake frame ratio.

III. Distributed Energy Beamforming Scheme

A. Hardware Architecture of Distributed Wireless Power Transmitters

In this subsection, we discuss the hardware architecture of distributed wireless power transmitters. Distributed wireless power transmitters are capable of controlling the phase and the magnitude of the transmit signal from each antenna. One possible architecture of the distributed wireless power transmitters is the centralized architecture in Fig. 7(a). In the centralized architecture, there is only one centralized entity that generates all transmit signals for all power beacons. The local oscillator generates a source signal which is amplified by the drive amplifier. The power splitter splits the amplified source signal into KN RF paths. In each path, the phase and the magnitude of the transmit signal are determined by the phase shifter and the variable gain amplifier, respectively. The phase shifters and the variable gain amplifiers are controlled by the controller. In the centralized architecture, the power beacons are simply formed by extending RF cables to the location of each power beacon. Although this centralized architecture is relatively easy to implement, it is not a truly distributed system. Moreover, the centralized architecture is difficult to install because of RF cables, and suffers from high power loss with lengthy RF cables.

In the semi-distributed architecture in Fig. 7(b), each power beacon is a stand-alone entity, each of which is almost identical to the centralized entity in the centralized architecture. Each power beacon independently generates a source signal by using its own local oscillator. Moreover, each power beacon

This article has been accepted for publication in a future issue of this journal, but has not been fully edited. Content may change prior to final publication. Citation information: DOI 10.1109/JIOT.2018.2790578, IEEE Internet of Things Journal

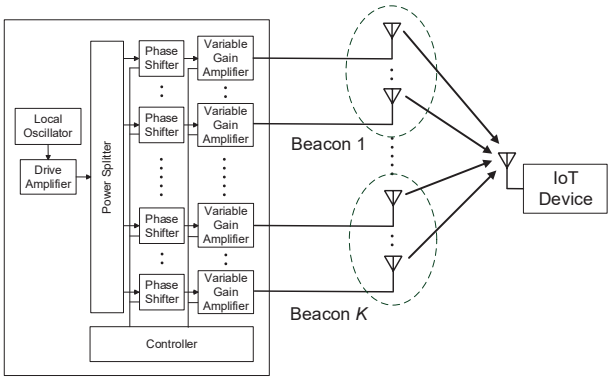

(a) Centralized architecture

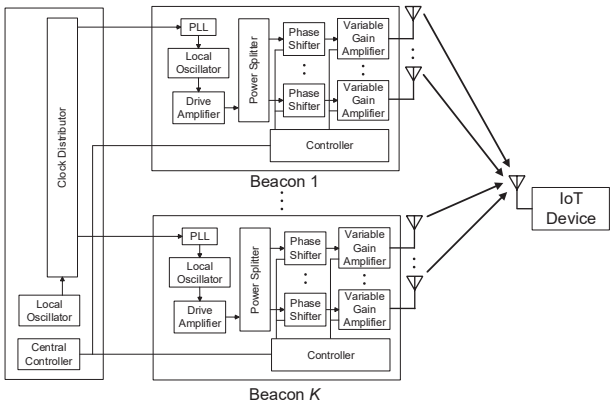

(b) Semi-distributed architecture

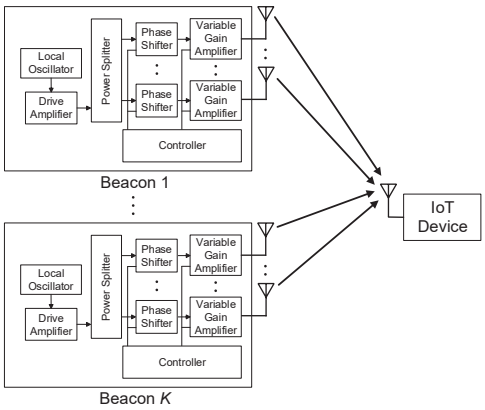

(c) Fully distributed architecture

Fig. 7. Hardware architectures of distributed wireless power transmitters.

has a separate controller to control the phases and the magnitudes of the transmit signals. The separate local oscillator and controller for each power beacon incur the frequency and phase synchronization problems.

Due to the imperfection in the local oscillator, the frequency of the source signal drifts from the nominal frequency configured in the oscillator. Moreover, the frequency of the source signal can be unstable and varying over time because of aging and environmental factors such as temperature. For example, if the short-term deviation of an oscillator with the nominal frequency of 1 GHz is 10^{-3} ppm for one second, the frequency of the oscillator can drift 1 Hz every second. Under this frequency drift, the frequencies of the source signals in different power beacons drift away from each other, and it is impossible to conduct optimal energy beamforming across the power beacons. In the semi-distributed architecture in Fig. 7(b), a common clock is provided to all power beacons by the central coordinator through cables to resolve the frequency synchronization problem. The low-frequency common clock is used as a reference clock for the phase-locked loop (PLL) to make the frequencies of the source signals of all power beacons synchronized.

The phase synchronization makes the phases of the RF signals from multiple antennas aligned at the receive antenna of the IoT device so that the receive power is maximized. Therefore, the phase synchronization is equivalent to the optimal beamforming. For the optimal beamforming, the channel gain between the transmit and receive antennas (i.e., $h_{k,n}$) should be estimated in the power beacon. Some channel gain estimation algorithms (e.g., [17]–[19]) have been proposed for the wireless power transfer. These channel gain estimation algorithms require a central coordinator that collects necessary information, performs computation, and controls the transmit signal from all antennas. For the phase synchronization, the semi-distributed architecture in Fig. 7(b) has a central coordinator with wired connections to all power beacons.

Although the semi-distributed architecture can achieve the frequency and phase synchronization, it is not a true distributed system because of the central coordinator connected to all power beacons by wires. Fig. 7(c) shows the fully distributed architecture without any central coordinator. This fully distributed architecture is easy to install compared to other architectures since it does not require any central coordinator or interconnected wire. However, it is hard to achieve the frequency and phase synchronization in this fully distributed architecture.

The following distributed frequency and phase synchronization methods can be applied to the fully distributed architecture. The authors of [20] have proposed a master-slave architecture for the distributed frequency synchronization, in which the slave nodes use the PLL to lock on the reference signal wirelessly broadcast by the master node. For the phase synchronization, a closed-loop one-bit feedback method is proposed in [21]. A time-slotted round-trip carrier synchronization protocol for the distributed beamforming is proposed in [22]. In [14], the authors have proposed a distributed wireless power transfer technique in which distributed energy transmitters adapt their transmit phases based on the energy feedback from the energy receiver. Although the above-mentioned methods can achieve the frequency and phase synchronization, it is actually costly and challenging to use these methods in a real system. Therefore, for the fully distributed architecture, we also consider the case that the frequency and phase synchronization across the power beacons is not available, as well as the case that it is available.

The protocols and algorithms for the frequency and phase synchronization in the fully distributed architecture are out of scope of this paper. In this paper, we focus on analyzing and

This article has been accepted for publication in a future issue of this journal, but has not been fully edited. Content may change prior to final publication. Citation information: DOI 10.1109/JIOT.2018.2790578, IEEE Internet of Things Journal

comparing the power transfer performances with or without the frequency and phase synchronization under the assumption that the above-mentioned synchronization methods are used.

B. Distributed Energy Beamforming Schemes

In this subsection, we explain the energy beamforming schemes for the distributed wireless power transmitter. We first introduce the transmit signal model in the transmitter architectures in Section III-A. The local oscillator generates the source signal with the nominal frequency f_c. Due to the imperfection of the oscillator circuit, a frequency drift can occur. Let $\Delta_k(t)$ denote a time-varying oscillator frequency drift of beacon k. Then, the RF source signal generated by the oscillator is

$$\mathrm{Re}\big[\exp\big(j2\pi\big(f_c t + \textstyle\int_0^t \Delta_k(\tau)\mathrm{d}\tau + \phi_k\big)\big], \tag{12}$$

where ϕ_k is the initial phase. From (12), the baseband source signal of beacon k is

$$o_k(t) = \exp\big(j2\pi\big(\textstyle\int_0^t \Delta_k(\tau)\mathrm{d}\tau + \phi_k\big)\big). \tag{13}$$

As explained in Section III-A, the frequency synchronization is achieved in the centralized or semi-distributed architecture. In the fully distributed architecture, it is possible to achieve the frequency synchronization if the wireless reference signal is available as explained in [20]. In the case that the oscillators are synchronized between the power beacons, all the power beacons have the same frequency offsets, that is, $\Delta_k(t) = \Delta(t)$ and $\phi_k = \phi$ for all $k = 1, \ldots, K$. Then, we have the same baseband source signals for all power beacons, i.e., $o(t) = o_k(t)$ for all k. On the other hand, the frequency is not synchronized in the fully distributed architecture without a wireless reference signal. In this case, $\Delta_k(t)$ is a process that independently varies over time for each power beacon k.

In a power beacon, the source signal is split into N transmit paths. In each transmit path, the phase and magnitude of the source signal are adjusted by the phase shifter and the variable gain amplifier, respectively. Let $s_{k,n}(t)$ denote a beamforming weight at time t. The beamforming weight is a complex number, which represents the phase shift and the magnitude of the signal transmitted from antenna n of beacon k. The beamforming weight vector of beacon k is denoted by $\mathbf{s}_k(t) = (s_{k,1}(t), \ldots, s_{k,N}(t))^T$. Then, the transmit signal vector from beacon k is

$$\mathbf{x}_k(t) = \mathbf{s}_k(t) o_k(t). \tag{14}$$

From (4), the receive signal at the IoT device is

$$y(t) = \sum_{k=1}^{K} \mathbf{h}_k^T \mathbf{x}_k(t) = \sum_{k=1}^{K} \mathbf{h}^T \mathbf{s}_k(t) o_k(t). \tag{15}$$

The receive power is $r(t) = |y(t)|^2/(2Z_0)$ as given in (5), and the average receive power is the time average of the receive power such that $\overline{r} = \langle r(t) \rangle$ as given in (10).

The distributed beamforming targets to maximize the average receive power $\overline{r}$ by controlling the beamforming weight vector $\mathbf{s}_k(t)$. The beamforming weight vector $\mathbf{s}_k(t)$ is decomposed as

$$\mathbf{s}_k(t) = \mathbf{w}_k(t) u_k(t) \sqrt{2Z_0 P}, \tag{16}$$

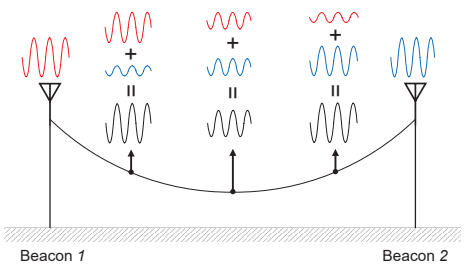

(a) Optimal beamforming

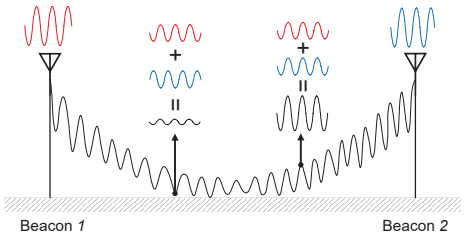

(b) Static beamforming

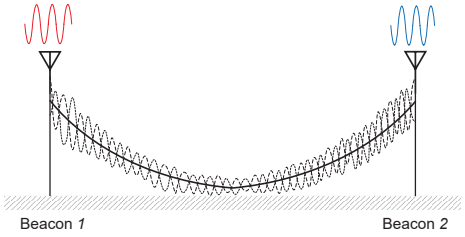

(c) Random beamforming

Fig. 8. Beamforming schemes.

where $\mathbf{w}_k(t) = (w_{k,1}(t), \ldots, w_{k,N}(t))^T$ is the intra-beacon beamforming weight vector and $u_k(t)$ is the inter-beacon beamforming weight. The power of the transmit signal from each antenna is fixed to P, and the intra-beacon and inter-beacon beamforming weights $w_{k,n}(t)$ and $u_k(t)$ have unit time-averaged power, that is, $\langle |w_{k,n}(t)|^2 \rangle = 1$ and $\langle |u_k(t)|^2 \rangle = 1$ for all k and n. Each power beacon decides the intra-beacon beamforming weights for beamforming among the antennas within the power beacon. The power beacons can cooperatively decide the inter-beacon beamforming weights for beamforming among the antennas in different power beacons.

We consider the optimal, static, and random beamforming schemes for both the intra-beacon and inter-beacon beamforming. Fig. 8 illustrates the concept of these beamforming schemes in the case that there are two power beacons each of which has a single antenna (i.e., $K = 2$ and $N = 1$). In this example, we fix the intra-beacon beamforming weights over time (i.e., $w_{1,1}(t) = 1$ and $w_{2,1}(t) = 1$) since there is only one antenna per power beacon. Fig. 8(a) shows the optimal beamforming scheme in which the transmit signals are optimally combined at the IoT device. To use the optimal beamforming scheme, the frequency synchronization is needed

This article has been accepted for publication in a future issue of this journal, but has not been fully edited. Content may change prior to final publication. Citation information: DOI 10.1109/JIOT.2018.2790578, IEEE Internet of Things Journal

(i.e., $o_1(t) = o_2(t)$), and the channel gains $h_{1,1}$ and $h_{2,1}$ should be estimated. The optimal beamforming scheme sets the beamforming weights to the conjugate of the channel gains, that is, $u_{1,1}(t) = h_{1,1}^*$ and $u_{2,1}(t) = h_{2,1}^*$.

We can use the static beamforming scheme as in Fig. 8(b) when the frequency synchronization is achieved but the channel gains are unknown. The beamforming weights are simply fixed over time in the static beamforming scheme, that is, $u_{1,1}(t) = u_{1,1}$ and $u_{2,1}(t) = u_{2,1}$. As can be seen in Fig. 8(b), the transmit signals from two antennas are destructively combined in many places, resulting in the spatial irregularity of the receive power. To avoid this problem, the random beamforming scheme can be used as in Fig. 8(c). In the random beamforming scheme, the beamforming weights $u_{1,1}(t)$ and $u_{2,1}(t)$ randomly vary over time for averaging out the spatial irregularity. This random beamforming scheme can also be used when the frequency synchronization is not achieved.

The optimal, static, and random beamforming schemes can be applied to the intra-beacon beamforming as follows.

- Optimal intra-beacon beamforming: If a power beacon can estimate the array response vector $\boldsymbol{\psi}_k$, it can perform the optimal intra-beacon beamforming. In this case, the intra-beacon beamforming weight vector is set to $\mathbf{w}_k(t) = \boldsymbol{\psi}_k^*$.
- Static intra-beacon beamforming: If the array response vector cannot be estimated, the power beacon can perform the static intra-beacon beamforming. The static intra-beacon beamforming statically sets $\mathbf{w}_k(t)$ to a fixed vector, that is, $\mathbf{w}_k(t) = \mathbf{w}_k$. Here, $\mathbf{w}_k$ is fixed over time, but is a random variable that is randomly decided at the start of transmission. The magnitude of $w_{k,n}$ is fixed to one (i.e., $|w_{k,n}| = 1$), and the phase of $w_{k,n}$ is uniformly distributed over 0 to 2π.
- Random intra-beacon beamforming: This beamforming scheme can be used when the array response vector cannot be estimated. In this beamforming scheme, $\mathbf{w}_k(t)$ randomly varies over time under the condition that $\langle w_{k,n}(t)\rangle = 0$, $\langle |w_{k,n}(t)|^2\rangle = 1$, and $\langle w_{k,n}(t) w_{k,m}(t)^*\rangle = 0$ for all n and m such that $n \neq m$.

We can apply the optimal, static, and random beamforming schemes to the inter-beacon beamforming as follows.

- Optimal inter-beacon beamforming: If the local oscillators in power beacons are synchronized and ξ_k's for $k = 1, \ldots, K$ can be estimated, the power beacons can cooperate with each other for the optimal inter-beacon beamforming. In this case, the inter-beacon beamforming weights are set to $u_k(t) = \xi_k^*$ for all $k = 1, \ldots, K$.
- Static inter-beacon beamforming: This beamforming scheme can be used when the local oscillators are synchronized but ξ_k's are unknown. In this scheme, $u_k(t)$ is fixed to a static value over time, that is, $u_k(t) = u_k$. The static value u_k is a random variable that is randomly decided at the start of transmission. The magnitude of u_k is fixed to one (i.e., $|u_k| = 1$), and the phase of u_k is uniformly distributed over 0 to 2π.
- Random inter-beacon beamforming: If the local oscillators are not synchronized or ξ_k's cannot be estimated, each power beacon can use a random inter-beacon beamforming to randomize the phase of the source signal. Then, $u_k(t)$ randomly varies over time under the condition that $\langle u_k(t)\rangle = 0$, $\langle |u_k(t)|^2\rangle = 1$, and $\langle u_k(t) u_l(t)^*\rangle = 0$ for all k and l such that $k \neq l$.

Many possible variations are realized according to which beamforming scheme is used for the inter-beacon and intra-beacon beamforming. In total, we have nine possible combinations of the inter-beacon and intra-beacon beamforming schemes.

IV. Analysis of Distributed Energy Beamforming

A. Average Receive Power Analysis

In the following, we analyze the average receive power at the IoT device for several meaningful combinations of the intra-beacon and inter-beacon beamforming schemes.

1) Optimal Intra-Beacon and Optimal Inter-Beacon Beamforming (i.e., Optimal Beamforming): In this scheme, the oscillator is synchronized between the power beacons, and the power beacons perform the optimal inter-beacon beamforming. In addition, each power beacon performs the optimal intra-beacon beamforming. Then, $\mathbf{w}_k(t) = \boldsymbol{\psi}_k^*$ and $u_k(t) = \xi_k^*$ for all $k = 1, \ldots, K$. The receive signal from beacon k is

$$\begin{aligned} y_k(t) &= \mathbf{h}^T \mathbf{s}_k(t) o_k(t) = (\zeta_k \xi_k \boldsymbol{\psi}_k)^T (\boldsymbol{\psi}_k^* \xi_k^* \sqrt{2Z_0 P}) o(t) \\ &= \zeta_k \sqrt{2Z_0 P} N o(t). \end{aligned} \tag{17}$$

Then, the average receive power is given by

$$\overline{r} = \frac{\langle |\sum_{k=1}^K y_k(t)|^2 \rangle}{2Z_0} = \Upsilon P N^2 \left(\sum_{k=1}^K d_k^{-\frac{\alpha}{2}} \right)^2. \tag{18}$$

2) Optimal Intra-Beacon and Random Inter-Beacon Beamforming (i.e., Optimal-Random Beamforming): This scheme corresponds to the case that each power beacon independently performs beamforming without any coordination between power beacons. The oscillators are not synchronized, and the inter-beacon beamforming weight is randomly varying over time. However, the intra-beacon beamforming is optimally conducted by each power beacon. Then, $\mathbf{w}_k(t) = \boldsymbol{\psi}_k^*$, and $u_k(t)$ is random. We can calculate the receive signal as

$$y_k(t) = \zeta_k \sqrt{2Z_0 P} N \xi_k u_k(t) o_k(t). \tag{19}$$

Then, the average receive power is

$$\begin{aligned} \overline{r} &= \Upsilon P N^2 \sum_{k=1}^K \sum_{l=1}^K d_k^{-\frac{\alpha}{2}} d_l^{-\frac{\alpha}{2}} \xi_k \xi_l^* \langle u_k(t) u_l^*(t) o_k(t) o_l^*(t) \rangle \\ &= \Upsilon P N^2 \sum_{k=1}^K d_k^{-\alpha}. \end{aligned} \tag{20}$$

This article has been accepted for publication in a future issue of this journal, but has not been fully edited. Content may change prior to final publication. Citation information: DOI 10.1109/JIOT.2018.2790578, IEEE Internet of Things Journal

3) Random Intra-Beacon and Random Inter-Beacon Beamforming (i.e., Random Beamforming): In this scheme, the oscillators are not synchronized, and the inter-beacon beamforming weights are randomly varying. Moreover, the power beacon is not equipped with the functionality to perform the optimal intra-beacon beamforming, and therefore, it randomizes the intra-beacon beamforming weights. Then, both $w_{k,n}(t)$ and $u_k(t)$ are random. In this case, the receive signal is

$$\begin{aligned} y_k(t) &= (\zeta_k \xi_k \boldsymbol{\psi}_k)^T (\boldsymbol{w}_k(t) u_k(t) \sqrt{2Z_0 P}) o_k(t) \\ &= \zeta_k \xi_k u_k(t) \sqrt{2Z_0 P} o_k(t) \boldsymbol{\psi}_k^T \boldsymbol{w}_k(t). \end{aligned} \tag{21}$$

From the receive signal, we can calculate the average receive power as

$$\begin{aligned} \overline{r} &= \Upsilon P \sum_{k=1}^{K} \sum_{l=1}^{K} d_k^{-\frac{\alpha}{2}} d_l^{-\frac{\alpha}{2}} \xi_k \xi_l^* \\ &\quad \times \langle u_k(t) u_l^*(t) o_k(t) o_l^*(t) \boldsymbol{\psi}_k^T \boldsymbol{w}_k(t) (\boldsymbol{\psi}_l^T \boldsymbol{w}_l(t))^* \rangle \\ &= \Upsilon P N \sum_{k=1}^{K} d_k^{-\alpha}. \end{aligned} \tag{22}$$

4) Static Intra-Beacon and Static Inter-Beacon Beamforming (i.e., Static Beamforming): In this scheme, the oscillators are synchronized, but the power beacons do not have the capability of the optimal inter-beacon or intra-beacon beamforming. The power beacons use fixed values over time for the inter-beacon and intra-beacon beamforming weights, that is, $\mathbf{w}_k(t) = \mathbf{w}_k$ and $u_k(t) = u_k$. Although $\mathbf{w}_k$ and u_k are fixed over time, those beamforming weights are considered as random variables that are randomly decided at the start of transmission. Then, we can calculate the receive signal as

$$y_k(t) = \zeta_k \xi_k u_k \sqrt{2Z_0 P} o(t) \boldsymbol{\psi}_k^T \boldsymbol{w}_k. \tag{23}$$

The average receive power is calculated as

$$\overline{r} = \Upsilon P \left| \sum_{k=1}^{K} \xi_k u_k \boldsymbol{\psi}_k^T \boldsymbol{w}_k d_k^{-\frac{\alpha}{2}} \right|^2. \tag{24}$$

Since u_k and $w_{k,n}$ are independent identically distributed random variables, $\xi_k u_k \boldsymbol{\psi}_k^T \boldsymbol{w}_k$ can be assumed to be a circularly symmetric Gaussian random variable with the variance of N if the number of antennas N is large enough. Under this assumption, $\sum_{k=1}^{K} \xi_k u_k \boldsymbol{\psi}_k^T \boldsymbol{w}_k d_k^{-\frac{\alpha}{2}}$ becomes a circularly symmetric Gaussian random variable with the variance of $N \sum_{k=1}^{K} d_k^{-\alpha}$. Then, the average receive power $\overline{r}$ becomes an exponentially distributed random variable with mean

$$m_{\overline{r}} = \mathbb{E}[\overline{r}] = \Upsilon P N \sum_{k=1}^{K} d_k^{-\alpha}. \tag{25}$$

B. Coverage Probability

The IoT device should receive a certain amount of power (i.e., $\overline{C}(\alpha)/\eta$) to support a given awake frame ratio α, as given in (11). Since the receive power is dependent upon the location of the IoT device according to the receive power analysis in Section IV-A, the IoT device can receive sufficient power at some locations while it cannot at other locations.

The coverage probability is defined as the probability that the receive power at the IoT device is not less than a given threshold. Let Δ denote the receive power threshold. Then, the coverage probability for the given receive power threshold is given by

$$Q(\Delta) = \Pr[\overline{r} \geq \Delta]. \tag{26}$$

We assume that each power beacon is placed at a fixed location. The coordinate of the IoT device (i.e., $\mathbf{c}$) is randomly distributed according to the uniform distribution within a confined area $\mathcal{A}$.

In the first three beamforming schemes analyzed in Sections IV-A (i.e., optimal, optimal-random, and random beamforming schemes), the average receive power is a deterministic variable. Let $\overline{r}(\mathbf{c})$ denote the average receive power when the IoT device is located at coordinate $\mathbf{c}$. Then, the coverage probability is

$$Q(\Delta) = \frac{\int_{\mathbf{c} \in \mathcal{A}} I(\overline{r}(\mathbf{c}) \geq \Delta) \, \mathrm{d}\mathbf{c}}{|\mathcal{A}|}, \tag{27}$$

where $I(x)$ is the indicator that is 1 if x is true; and 0 otherwise, and $|\mathcal{A}|$ is the area of $\mathcal{A}$.

On the other hand, if the static beamforming is used, the average receive power follows an exponential distribution. Let $m_{\overline{r}}(\mathbf{c})$ as the mean of the average receive power when the receiver is located at $\mathbf{c}$. Then, the coverage probability is

$$Q(\Delta) = \frac{\int_{\mathbf{c} \in \mathcal{A}} \exp(-\Delta / m_{\overline{r}}(\mathbf{c})) \, \mathrm{d}\mathbf{c}}{|\mathcal{A}|}. \tag{28}$$

V. Numerical Results

A. Testbed and Simulation Setup

We have built a real-time testbed to conduct experiments on the distributed beamforming schemes. For the power beacon, we have fabricated an RF phased array board that consists of 16 transmit paths, as shown in Fig. 10(a). In this phased array board, the power splitter divides the source signal into 16 transmit paths. Each transmit path consists of a phase shifter, a variable attenuator, and a power amplifier. The phase shifter and the variable attenuator are controlled by the voltage from the onboard digital-to-analog conversion (DAC) chip.

Fig. 10(b) shows the devices that control the phased array board and provide the source signal. We use a field programmable gate array (FPGA) device (i.e., NI PXI-7841R) to control the phased array board through the DAC chip. The source RF signal is provided to the phased array board by using a signal generator (i.e., TSG4100A) and a drive amplifier (i.e., Mini-Circuits ZHL-5W-422+). The RF signal from each output port of the phased array board is delivered to a dipole antenna with a 3 dBi antenna gain through a 6-meter cable. The RF signal is a CW with the carrier frequency of $f_c = 920$ MHz. The transmit power from each antenna is set to $P = 168$ mW. The power beacon based on the phased array board is similar to the centralized architecture shown in Fig. 7(a). Although the frequency and phase synchronization can be achieved in this architecture, we also emulate the scenarios in which the frequency or phase synchronization is not available.

This article has been accepted for publication in a future issue of this journal, but has not been fully edited. Content may change prior to final publication. Citation information: DOI 10.1109/JIOT.2018.2790578, IEEE Internet of Things Journal

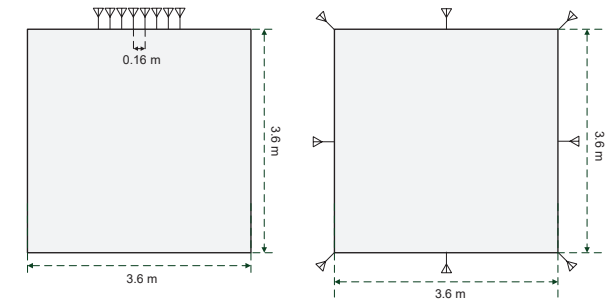

(a) B1A8 formation (b) B8A1 formation

(c) B4A4 formation (d) B8A2 formation

Fig. 9. Testbed layout.

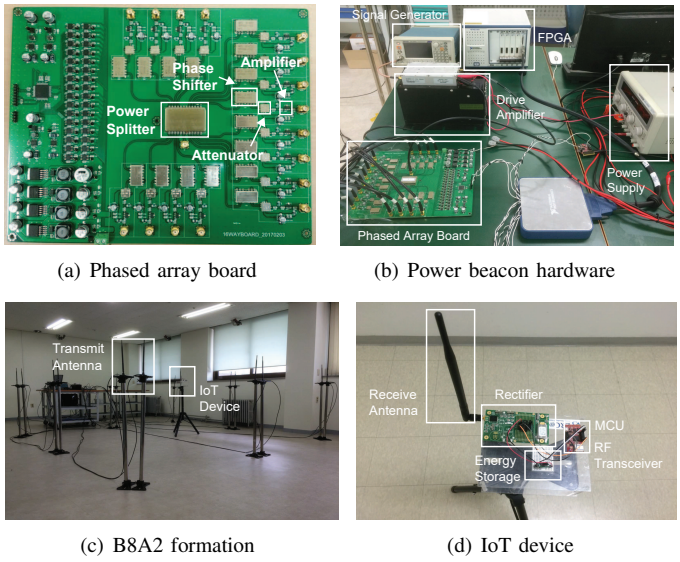

(a) Phased array board (b) Power beacon hardware

(c) B8A2 formation (d) IoT device

Fig. 10. Distributed wireless power transfer testbed.

We show the testbed layout and picture in Figs. 9 and 10, respectively. The testbed space is a 3.6m-by-3.6m square area. We consider four different power beacon formations as shown in Fig. 9. We use the term "BKAN formation" for referring to the power beacon formation with K power beacons each of which is equipped with N antennas. Fig. 10(c) shows the example picture of the B8A2 formation in our testbed.

The IoT device consists of the Powercast P1110 board, the energy storage, and the Zolertia Z1 mote, as shown in Fig. 10(d). The Powercast P1110 board is used for receiving power from the power beacons, including the rectifier, power management, and power sensor circuits. We use a supercapacitor (i.e., Samxon DDL series) as the energy storage. The Zolertia Z1 mote adopts TI MSP430 as an MCU and TI CC2420 as an RF transceiver. The RF transceiver CC2420 uses the 802.15.4 protocol on the 2.4 GHz frequency band. In the Zolertia Z1 mote, we use a Contiki operating system (OS) as a software platform. The receive power at the receive antenna is measured by the IoT device, which is then reported to the power beacon by the RF transceiver.

For the optimal beamforming, the testbed utilizes the channel estimation algorithm proposed in our previous work [23]. This channel estimation algorithm is able to obtain the channel gains between all the transmit antennas and the receive antenna based on the receive power measurement at the IoT device. The channel estimation algorithm is not described in more detail since it is out of the scope of this paper. It is noted that the channel estimation algorithm in [23] can incur extra power consumption of the IoT device for measuring and reporting the receive power.

We have also conducted simulations by using Matlab in the same system model as that for the experiments. In this simulation, we use the simple channel gain model in (6) to simulate the channel gains between the transmit and receive antennas. For the random and optimal-random beamforming schemes, we have generated 100 signals with random phases for the beamforming weights, and have calculated the average of the receive power.

B. Experimental, Simulation, and Analytical Results

Figs. 11–18 show the heat maps of the receive power over the testbed area for each formation, which are, respectively, obtained by the experiments and the simulations. For each heat map based on the experiment, we have measured the receive power at around 1,400 sample positions for accurately reconstructing a real receive power map. Recall that, in the static beamforming, the intra-beacon and inter-beacon beamforming weights are fixed to static values over time, but these static values are randomly decided at the start of transmission. In the experiment for the static beamforming, we have done the test only for the case that the static values are all ones (i.e., $u_k(t) = 1$ and $w_{k,n}(t) = 1$ for all k and n).

In all Figs. 11–18, it can be seen that the experimental results are very similar to the simulation results. However, we can observe more irregular patterns in the experimental results, which is mainly caused by the multipath propagation environment in the real testbed. The simple channel gain model in (6), which is used for the simulation, does not take into account the multipath propagation environment, although we have used the empirically-obtained parameters.

Figs. 11 and 12 show the heat map when only one power beacon with 8 antennas is placed (i.e., B1A8 formation). In these figures, we can see that only the IoT device close to the power beacon can enjoy high receive power, while the receive power rapidly decreases as the IoT device is moved away from the power beacon. Therefore, the B1A8 formation does not evenly supply power over the whole target area. In addition, we can see that the optimal beamforming yields much higher power than the random beamforming does, while the general shape of the heat maps are similar. In the static beamforming

This article has been accepted for publication in a future issue of this journal, but has not been fully edited. Content may change prior to final publication. Citation information: DOI 10.1109/JIOT.2018.2790578, IEEE Internet of Things Journal

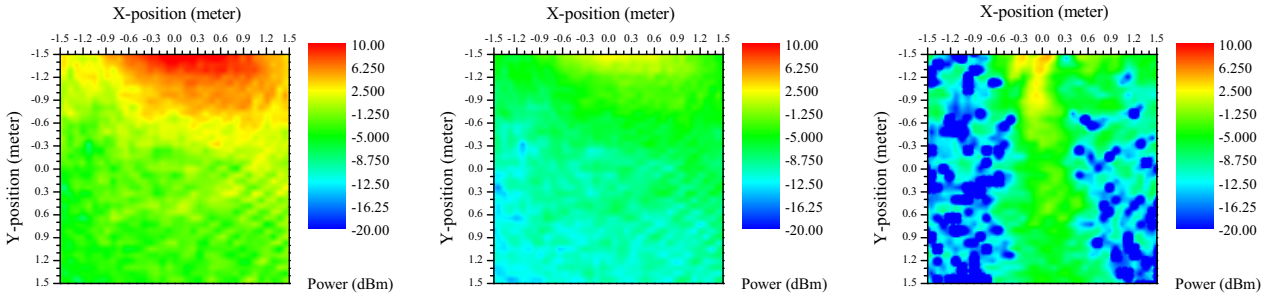

(a) Optimal (b) Random (c) Static

Fig. 11. Experimental results of receive power heat maps in B1A8 formation.

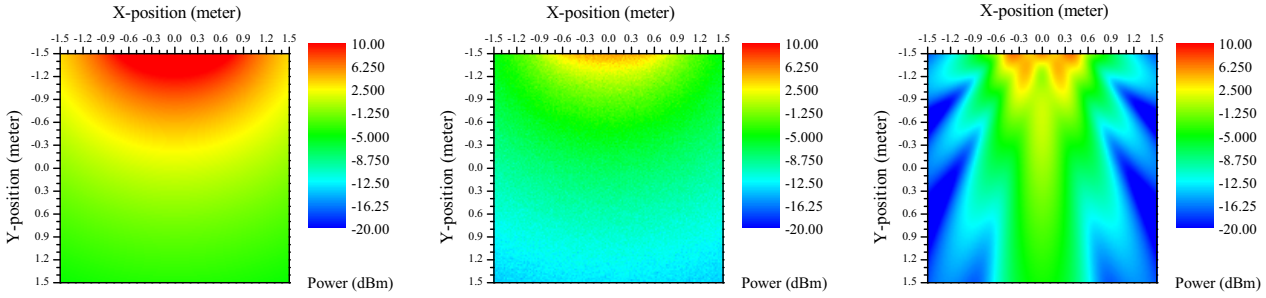

(a) Optimal (b) Random (c) Static

Fig. 12. Simulation results of receive power heat maps in B1A8 formation.

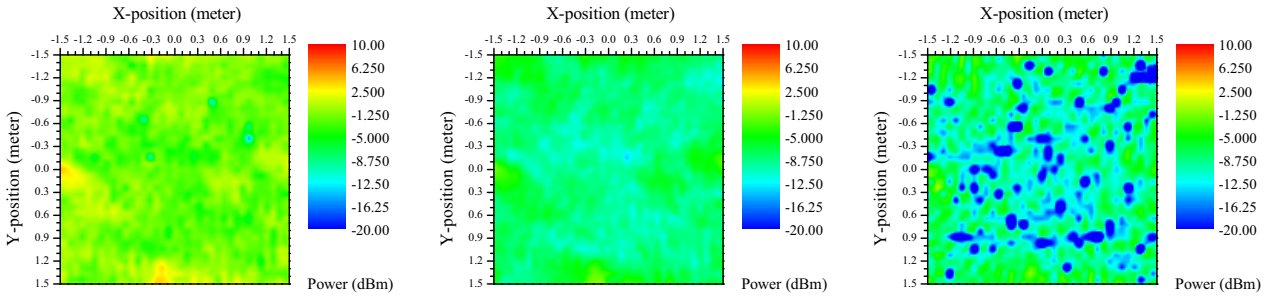

(a) Optimal (b) Random (c) Static

Fig. 13. Experimental results of receive power heat maps in B8A1 formation.

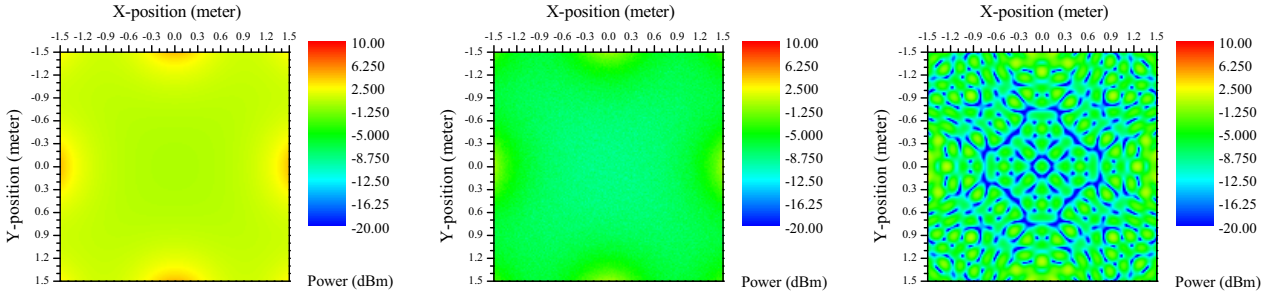

(a) Optimal (b) Random (c) Static

Fig. 14. Simulation results of receive power heat maps in B8A1 formation.

This article has been accepted for publication in a future issue of this journal, but has not been fully edited. Content may change prior to final publication. Citation information: DOI 10.1109/JIOT.2018.2790578, IEEE Internet of Things Journal

case, we can see that an RF beam is formed in both the experimental and simulation results, since the same phases are excited in all transmit antennas. The IoT device outside of the RF beam can only receive very small power since the RF signals from multiple antennas are destructively combined in such places.

In Figs. 13 and 14, the heat map of the receive power in the case of the B8A1 formation is shown. In contrast to the B1A8 formation, the whole testbed area is surrounded by 8 antennas in the B8A1 formation. As a result, we can observe that the receive power is evenly distributed over the whole area in the optimal and random beamforming cases. Therefore, it is expected that the B8A1 formation is more advantageous than the B1A8 formation in terms of the coverage probability when the receive power threshold is moderately set. In the static beamforming case, we can observe that the heat map is riddled with "holes" with very low receive power, where the RF signals are destructively combined. This means that a lot of blind spots of no power supply can arise if the static beamforming is used.

Figs. 15–18 show the heat map in the cases of the B4A4 and B8A2 formations, respectively. In these formations, we also present the optimal-random beamforming case in which the optimal beamforming is performed within each power beacon, but the phases of different power beacons are randomized due to the lack of cooperation between power beacons. As expected, the performance of the optimal-random beamforming is somewhere in between those of the optimal and the random beamforming schemes. With the number of transmit antennas twice higher than that of the B1A8 and B8A1 formations, the optimal beamforming in the B4A4 and B8A2 formations is able to cover the whole testbed area with quite high receive power.

In Figs. 19 and 20, we show the coverage probability, which is defined as the probability of the receive power no less than a given receive power threshold. These graphs show the coverage probability for the given receive power threshold on the x-axis. The coverage probability from the experiments are shown Figs. 19, while that from the simulation and the analysis are shown in Fig. 20. In Fig. 20, the simulation and the analytical results are, respectively, denoted by "Sim" and "An". The coverage probabilities from the experiments and the simulations are obtained based on their respective heat maps of the receive power. On the other hand, the analysis results of the coverage probability are derived from the simple equations introduced in Section IV.

In Figs. 19 and 20, we can see that the experimental results very well matches with the simulation and analytical results for all formations and beamforming schemes, in spite of the simplified channel model for the simulation and the analysis. This means that the simple analytic equations in Section IV can be used for predicting the coverage probability before actually developing and installing the distributed wireless power transfer systems with various beamforming schemes.

In these figures, we can see that the receive power distribution of the B1A8 formation is more dispersed than that of the B8A1 formation since the IoT device close to the only power beacon in the B1A8 formation can receive high power while that far from the power beacon receives very small power. This leads to the potential benefit of using many spatially distributed power beacons with a smaller number of antennas over using one power beacon with many antennas, when the receive power threshold is moderately low. For example, in the experimental results in Figs. 19(a) and 19(b), if the optimal beamforming is used and the receive power threshold is -3 dBm, the coverage probability of the B8A1 formation is around 0.85 while that of the B1A8 formation is around 0.75. In the analytical results in Figs. 20(a) and 20(b), this performance gap is shown to be much bigger, that is, if the receive power threshold is 0 dBm, the coverage probability of the B8A1 formation is close to 1 while that of the B1A8 formation is around 0.55. If the inter-beacon beamforming is not available, this advantage of using spatially distributed power beacons may not be attained because of the large performance gap between the optimal and random beamforming schemes.

These figures also show the disadvantage of the static beamforming. We can see that, if the static beamforming is used, there are many places where the receive power is very low due to the destructive combination of the RF signals. Therefore, if the optimal beamforming is not available, it would be better to randomize the phases of the transmit signals to average out the receive power.

VI. Conclusion

In this paper, we have suggested the potential architectures of the distributed wireless power transfer system, and have investigated the phase and frequency synchronization problems that might arise in the distributed architecture. We have analyzed the receive power according to various intra-beacon and inter-beacon beamforming schemes. We have also conducted extensive experiments on a real testbed to see how the receive power is distributed within a confined area. We have shown that the experiment results very well agree with the analytical results, which proves the usefulness of the proposed analytic formula in designing the distributed wireless power transfer system. The experimental results show that using spatially distributed power beacons with a single antenna can be advantageous over using a single power beacon with many antennas in terms of the coverage probability. However, this advantage is achieved only when the optimal inter-beacon beamforming can be realized in the distributed antenna system. The optimal inter-beacon beamforming requires the frequency synchronization in the oscillators as well as the beamforming coordinations between different power beacons. Therefore, further research on the optimal inter-beacon beamforming schemes should be done to realize the full potential of the distributed wireless power transfer system.

For expediting the adoption of the RF wireless power transfer in the practical IoT systems, it is very crucial to extend the coverage area of the wireless power transfer with sufficiently high power transfer efficiency so that the wireless power transfer can be applied to the wide range of IoT applications. The proposed distributed wireless power transfer along with the beamforming is a strong enabling candidate technology for

This article has been accepted for publication in a future issue of this journal, but has not been fully edited. Content may change prior to final publication. Citation information: DOI 10.1109/JIOT.2018.2790578, IEEE Internet of Things Journal

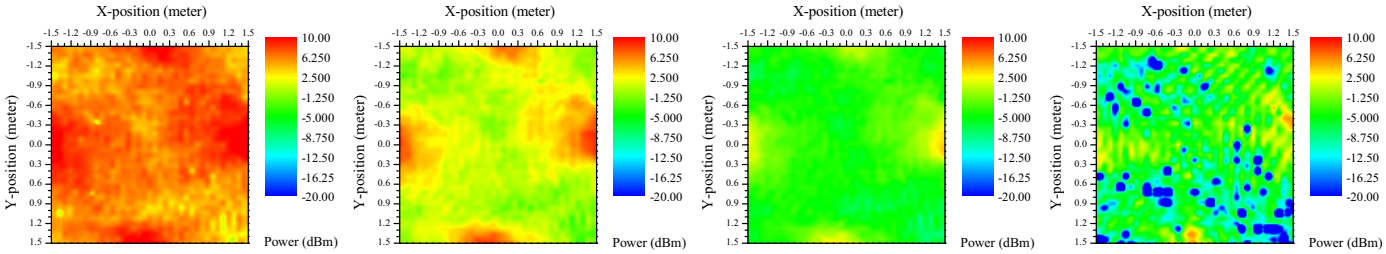

(a) Optimal (b) Optimal-random (c) Random (d) Static

Fig. 15. Experimental results of receive power heat maps in B4A4 formation.

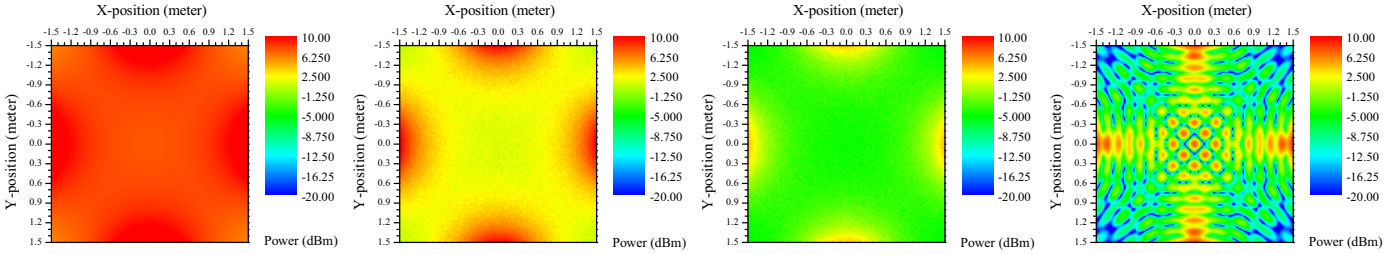

(a) Optimal (b) Optimal-random (c) Random (d) Static

Fig. 16. Simulation results of receive power heat maps in B4A4 formation.

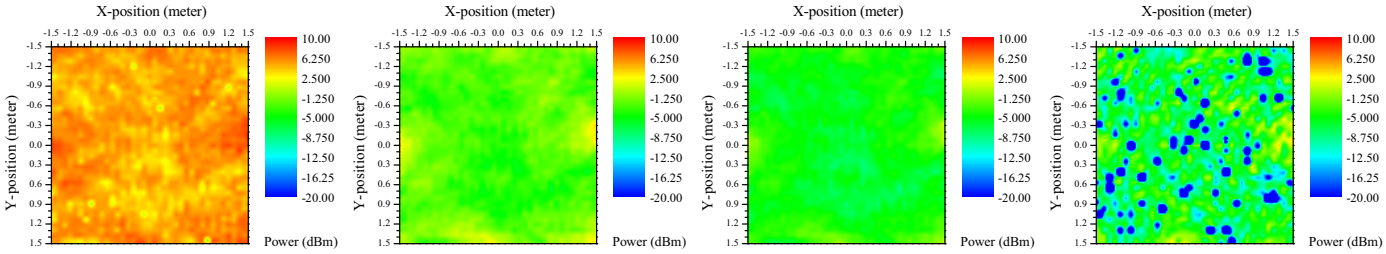

(a) Optimal (b) Optimal-random (c) Random (d) Static

Fig. 17. Experimental results of receive power heat maps in B8A2 formation.

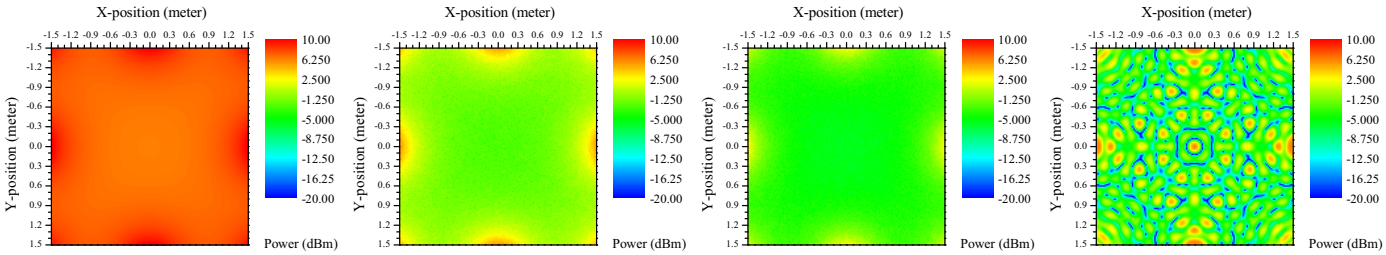

(a) Optimal (b) Optimal-random (c) Random (d) Static

Fig. 18. Simulation results of receive power heat maps in B8A2 formation.

This article has been accepted for publication in a future issue of this journal, but has not been fully edited. Content may change prior to final publication. Citation information: DOI 10.1109/JIOT.2018.2790578, IEEE Internet of Things Journal

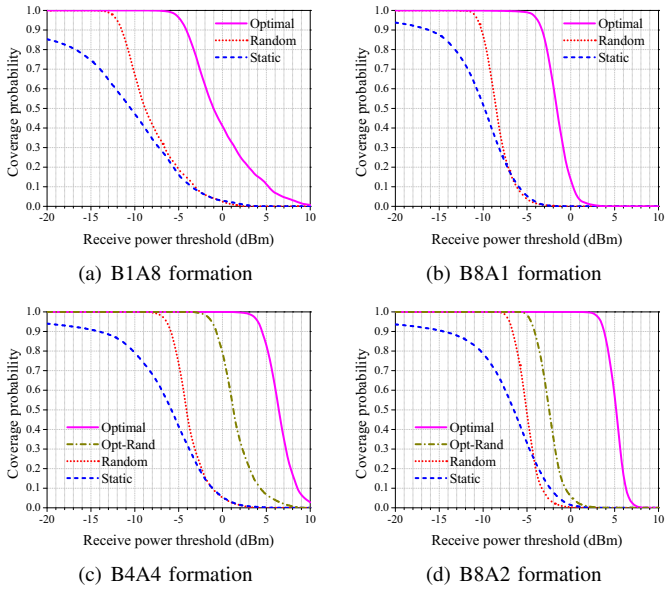

(a) B1A8 formation (b) B8A1 formation

(c) B4A4 formation (d) B8A2 formation

Fig. 19. Experimental results of coverage probability.

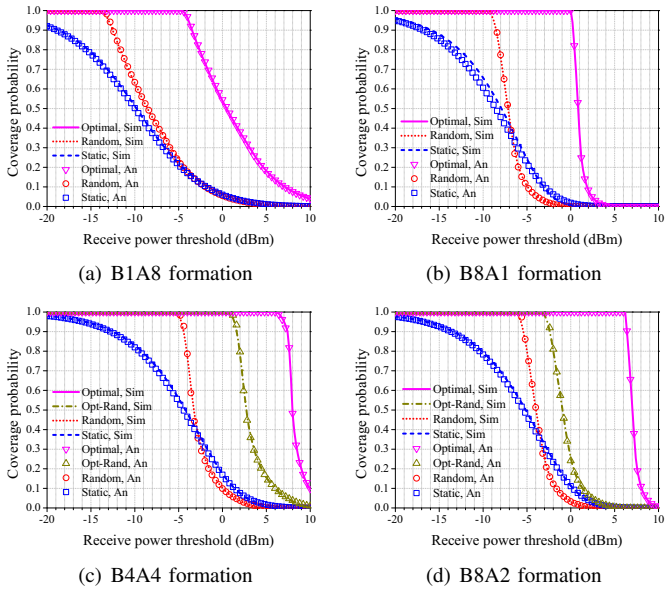

(a) B1A8 formation (b) B8A1 formation

(c) B4A4 formation (d) B8A2 formation

Fig. 20. Simulation and analytical results of coverage probability.

accommodating a large area supplied with wireless power. It is envisioned that more researches and experimental trials on this topic will eventually realize the practical battery-less IoT systems based on the RF wireless power transfer.

REFERENCES

[1] Y. Zeng, B. Clerckx, and R. Zhang, "Communications and signals design for wireless power transmission," *IEEE Trans. Commun.*, vol. 65, no. 5, pp. 2264–2290, May 2017.

[2] I. Krikidis, S. Timotheou, S. Nikolaou, G. Zheng, D. W. K. Ng, and R. Schober, "Simultaneous wireless information and power transfer in modern communication systems," *IEEE Commun. Mag.*, vol. 52, no. 11, pp. 104–110, Nov. 2014.

[3] K. Huang, C. Zhong, and G. Zhu, "Some new research trends in wirelessly powered communications," *IEEE Wireless Commun.*, vol. 23, no. 2, pp. 19–27, Apr. 2016.

[4] F. Yuan, S. Jin, K.-K. Wong, J. Zhao, and H. Zhu, "Wireless information and power transfer design for energy cooperation distributed antenna systems," *IEEE Access*, vol. 5, pp. 8094–8105, 2017.

[5] D. W. K. Ng and R. Schober, "Secure and green SWIPT in distributed antenna networks with limited backhaul capacity," *IEEE Trans. Wireless Commun.*, vol. 14, no. 9, pp. 5082–5097, Sep. 2015.

[6] S. Lee, L. Liu, and R. Zhang, "Collaborative wireless energy and information transfer in interference channel," *IEEE Trans. Wireless Commun.*, vol. 14, no. 1, pp. 545–557, Jan. 2015.

[7] F. Yuan, S. Jin, Y. Huang, K. Wong, Q. T. Zhang, and H. Zhu, "Joint wireless information and energy transfer in massive distributed antenna systems," *IEEE Commun. Mag.*, vol. 53, no. 6, pp. 109–116, Jun. 2015.

[8] N. Shinohara, T. Mitani, and H. Matsumoto, "Study on ubiquitous power source with microwave power transmission," in *Proc. Int. Union Radio Sci. (URSI) Gen. Assem. 2005*, New Delhi, India, Oct. 2005.

[9] J. He, X. Wang, L. Guo, S. Shen, and M. Lu, "A distributed retro-reflective beamformer for wireless power transmission," *Microw. Opt. Technol. Lett.*, vol. 57, no. 8, pp. 1873–1876, Aug. 2015.

[10] M. Y. Naderi, K. R. Chowdhury, S. Basagni, W. Heinzelman, S. De, and S. Jana, "Experimental study of concurrent data and wireless energy transfer for sensor networks," in *Proc. IEEE GLOBECOM 2014*, Austin, Tx, Dec. 2014.

[11] M. Y. Naderi, P. Nintanavongsa, and K. R. Chowdhury, "RF-MAC: A medium access control protocol for re-chargeable sensor networks powered by wireless energy harvesting," *IEEE Trans. Wireless Commun.*, vol. 13, no. 7, pp. 3926–3937, Jul. 2014.

[12] D. Maehara, G. K. Tran, K. Sakaguchi, and K. Araki, "Experimental study on battery-less sensor network activated by multi-point wireless energy transmission," *IEICE Trans. Commun.*, vol. E99-B, no. 4, pp. 905–916, Apr. 2016.

[13] R. Mudumbai, D. R. B. III, U. Madhow, and H. V. Poor, "Distributed transmit beamforming: challenges and recent progress," *IEEE Commun. Mag.*, vol. 47, no. 2, pp. 102–110, Feb. 2009.

[14] S. Lee and R. Zhang, "Distributed wireless power transfer with energy feedback," *IEEE Trans. Signal Process.*, vol. 65, no. 7, pp. 1685–1699, Apr. 2017.

[15] K. W. Choi, L. Ginting, D. Setiawan, A. A. Aziz, and D. I. Kim, "Coverage probability of distributed wireless power transfer system," in *Proc. ICUFN 2017*, Milan, Italy, Jul. 2017.

[16] E. Boshkovska, D. W. K. Ng, N. Zlatanov, and R. Schober, "Practical non-linear energy harvesting model and resource allocation for SWIPT systems," *IEEE Commun. Lett.*, vol. 19, no. 12, pp. 2082–2085, Dec. 2015.

[17] Y. Zeng and R. Zhang, "Optimized training design for wireless energy transfer," *IEEE Trans. Commun.*, vol. 63, no. 2, pp. 536–550, Feb. 2015.

[18] J. Xu and R. Zhang, "Energy beamforming with one-bit feedback," *IEEE Trans. Signal Process.*, vol. 62, no. 20, pp. 5370–5381, Oct. 2014.

[19] K. W. Choi, D. I. Kim, and M. Y. Chung, "Received power-based channel estimation for energy beamforming in multiple-antenna RF energy transfer system," *IEEE Trans. Signal Process.*, vol. 65, no. 6, pp. 1461–1476, Mar. 2017.

[20] R. Mudumbai, G. Barriac, and U. Madhow, "On the feasibility of distributed beamforming in wireless networks," *IEEE Trans. Wireless Commun.*, vol. 6, no. 5, pp. 1754–1763, May 2007.

[21] R. Mudumbai, B. Wild, U. Madhow, and K. Ramchandran, "Distributed beamforming using 1 bit feedback: from concept to realization," in *Proc. Allerton Conference on Communication Control and Computing 2006*, Monticello, IL, 2006.

[22] D. R. B. III and H. V. Poor, "Time-slotted round-trip carrier synchronization for distributed beamforming," vol. 56, no. 11, pp. 5630–5643, Nov. 2008.

[23] K. W. Choi, P. A. Rosyady, L. Ginting, A. A. Aziz, and D. I. Kim, "Wireless-powered sensor networks: How to realize," *IEEE Trans. Wireless Commun.*, vol. 16, no. 1, pp. 221–234, Jan. 2017.